Supporting Information

Kremien et al. 10.1073/pnas.1301826110

SI Mass Transfer Coefficient

Mass balance modeling was applied to quantify the contribution of pulsation to the increase of oxygen fluxes across the coral surface and to evaluate its impact on photosynthesis. The model assumes fully mixed conditions in the sealed metabolic chamber aquarium, a uniform oxygen flux across the coral surface, and that the flux can be modeled using a mass transfer coefficient formulation. The chamber oxygen concentration, $C(t)$, measured with the oxygen optode was modeled by the following balance differential equation:

$$\frac{V}{A}\frac{\partial C}{\partial t} = L\left(C_c - C(t)\right), \qquad \textbf{[S1]}$$

where L is the mass transfer coefficient and C_c is the oxygen concentration inside the coral tissue, such that the oxygen flux from the coral to the ambient water is modeled as $L(C_c - C(t))$. A is the coral surface, V is the chamber volume, and t is time. Eq. **S1** was solved analytically given an initial oxygen concentration of $C(0) = C_0$:

$$\frac{C(t) - C_c}{C_0 - C_c} = e^{-\frac{AL}{V}t}. \qquad \textbf{[S2]}$$

Fig. S3 presents our experimental results for the three corals (colored symbols) and the exponential curve of Eq. **S2** in its dimensionless form (as a continuous line). Note that V and A were measured parameters, whereas C_c and L were computed through a curve fitting procedure (for values, see Table S3). Generally, the fit is good for all data points, suggesting that this model represents the oxygen dynamics in our experiments. The parameters obtained from this fit indicate that the mass transfer coefficient (L) is 9.42 ± 2.46 (mean ± SD) times larger during pulsation relative to rest, reassuring our finding that pulsation renders a remarkable augmentation of the oxygen production rates by *Heteroxenia fuscescens* (Fig. 4). The values obtained for the oxygen concentration inside the coral tissue (C_c) are lower by 75–200 μmol·L^{-1} in pulsating conditions than in nonpulsating colonies (Table S3), indicating that pulsation maintains a decreased oxygen concentration in the coral tissue, thereby enhancing photosynthesis rates. Moreover, the C_c values are of the same range as measured with microelectrodes in stony corals, algae, and sea grasses (1), another indication that our model is compatible with the natural system.

SI Mixing Intensity Analysis

To explore the mixing induced by pulsation, we decomposed the raw instantaneous velocity as follows: the two velocity components, u and w, were defined as the sum of three velocity contributions: the current velocity, u_c and w_c; the wave orbital velocity, u_w and w_w; and the turbulent velocity, u_t and w_t.

$$u(t) = u_c(t) + u_w(t) + u_t(t) \qquad w(t) = w_c(t) + w_w(t) + w_t(t). \qquad \textbf{[S3]}$$

The decomposition of the velocity components $u(t)$ and $w(t)$ was obtained at each location within the velocity field by applying a fast Fourier transform (FFT) filter in the frequency domain and then recovering the time domain signal of the three components of the decomposed velocity. The main difficulty in this decomposition was the potential overlap of the wave and turbulence frequency ranges. However, we found that our data could be decomposed with a small uncertainty, as the sensitivity of the decomposition to the choice of the current, wave, and turbulent frequency cutoffs was small. Yet we acknowledge that the particular choice for velocity component is subjective and only general trends can be obtained when applying this FFT filtering. Note that we examined the realizations of each set individually and chose its frequency ranges separately. We then used this choice of frequency ranges for all of the measurement locations within the velocity field from the top of the measurement domain to the coral polyps. Although this may generate a bias because the polyps–flow interaction may add and remove some of the flow frequencies, the distinguished lower frequency of the waves allow us to assume that the u_t and w_t velocities contain both the flow turbulence and the effect of the polyps on the flow. The turbulence intensity is presented (Fig. 6) as the normalized mean square velocity $(\overline{u_t^2} + \overline{w_t^2})/(\overline{u}^2 + \overline{w}^2)$ at each location in the measurement domain.

SI Materials and Methods

Underwater Particle Image Velocimetry. Underwater particle image velocimetry (UPIV) measurements of the soft coral *H. fuscescens* were taken when the polyps were pulsating, followed by identical measurements after a diver gently touched the polyps, inducing a resting state that lasted a few minutes. The measurements were carried out at night with divers verifying the pulsation/resting state before each measurement set. Records consisted of several sets, each consisting of 50–100 image pairs (10–20 s). On one occasion, we managed to obtain a set during an intermediate state—when the coral tentacles were fully extended but pulsation not yet started. This rare record was used to examine the contribution of the pulsating motion by itself, not confounded by the usual co-occurrence of extended morphology and pulsation motion. Several cycles of pulsation and rest were recorded each night, allowing us to obtain sets of data in different flow velocities. Table S2 lists the information about the sets recorded during this study. Each image pair generated about 1,300 velocity vectors calculated using a custom-modified version of MatPIV (version 1.6.1) (2). Cross-correlation was used through a multipass mode in all cases. The dimensions of the square interrogation areas in these passes were 512 × 512, 256 × 256, 128 × 128, and 64 × 64 pixels with two passes on each dimension. An overlap of 50% was applied, resulting in a distance between neighboring velocity vectors of 0.6 mm. Each velocity vector was examined using first a global filter (with $2.5 < g < 3.5$, where g is the number of SDs of the entire instantaneous vector field ensemble, calculated relative to its mean) and then, when necessary, a local filter (with l = 5, where l is the number of SDs around the median value of $n = (3 \times 3 - 1)$ neighboring vectors, calculated using a kernel weighting scheme). When the velocity vector was marked as an outlier, it was rejected and then replaced by a kernel interpolation of the nearby velocity vectors.

The velocity vector at a given point is defined as follows: $\vec{V}(t) = u(t)\hat{i} + v(t)\hat{j} + w(t)\hat{k}$. The PIV measurements were obtained in a vertical plane, and thus only u and w were measured. The x–z measurement plane was defined so that x is positive toward the south and z is positive upward. To avoid the polyps' destruction on the analysis, all measurements took place on the section immediately above the active/not active polyps (Fig. S1). For each set individually, the origin $(x, z) = (0, 0)$ was defined at the tip of the uppermost polyp seen in the frame. In order for our measurements to be taken at the section immediately above active and resting polyps, the position of the UPIV camera was

finely tuned (up to 1 cm in elevation) based on the position of the tentacles at that time.

An ensemble average (3) was used for temporal averaging of the two instantaneous velocity components, $u(x, z, t)$ and $w(x, z, t)$ as follows:

$$\overline{u} = \frac{1}{N}\sum_{i=1}^{N} u_i; \qquad \overline{w} = \frac{1}{N}\sum_{i=1}^{N} w_i, \qquad \textbf{[S4]}$$

where N is the number of realizations in each set. In addition, the vertical profiles of the horizontal and the vertical mean velocity components $\langle\overline{u}\rangle_x(z)$ and $\langle\overline{w}\rangle_x(z)$, respectively, were obtained by spatially averaging $\overline{u}$ and $\overline{w}$ along the x coordinate.

A Lagrangian approach based on tracking imaginary particles in our flow records was used to examine whether polyp pulsation reduces the probability of water (and as a result solutes and particles) being refiltered by the coral. Each trajectory started at the lowest boundary of our measurement domain (i.e., adjacent to coral surface). We assumed that the starting point was sufficiently close to the coral tissue to allow an uptake of waterborne commodities (e.g., dissolved organic matter, nutrients, oxygen, CO_2) from the water at that point. Then the imaginary particle was allowed to move in time steps of 0.2 s according to the vectors measured by the UPIV at each point, as follows:

$$X(t+dt) = X(t) + dt\cdot u(x,z,t), \quad Z(t+dt) = Z(t) + dt\cdot w(x,z,t), \qquad \textbf{[S5]}$$

where $dt = 0.2$ s is the time step imposed by the sampling frequency. This Lagrangian deterministic procedure was repeated until the particle exited the measurement domain. The entire tracking simulation was repeated for each data point along the domain's bottom boundary (n = 42 points). The simulation was repeated ~50 times for each of the 42 points, advancing the start point in steps of 0.2 s. Tracks with less than five steps were discarded as it was found that they do not represent realistic trajectories. Because the calculated locations (X, Z) were typically found in-between PIV measurement data points (0.6 mm apart), an interpolation was used to calculate the velocity vector at that point, assuming a smooth polynomial change between each two data points.

1. Mass T, Genin A, Shavit U, Grinstein M, Tchernov D (2010) Flow enhances photosynthesis in marine benthic autotrophs by increasing the efflux of oxygen from the organism to the water. *Proc Natl Acad Sci USA* 107(6):2527–2531.
2. Sveen JK (2004) *An Introduction to MatPIV, version 1.6.1* (Department of Math, University of Oslo, Oslo).
3. Pope SB (2000) *Turbulent Flows* (Cambridge Univ, Cambridge, UK).

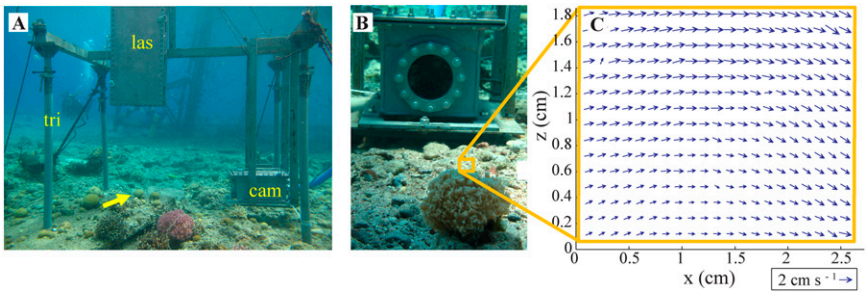

Fig. S1. The underwater particle image velocimetry system (UPIV) at 5-m depth in the coral reef of Eilat. (*A*) A general view of the UPIV system: cam, camera (in housing); las, laser (in housing); tri, tripod. The arrow indicates the target coral. (*B*) A close-up photograph showing the UPIV camera orientated on *H. fuscescens*. The orange square indicates the measurement domain included in the UPIV images. (*C*) Sample vector map of the instantaneous velocity field. The direction of x is positive into the page corresponding to *A* and z points upward. For clarity, only one out of four vectors is shown.

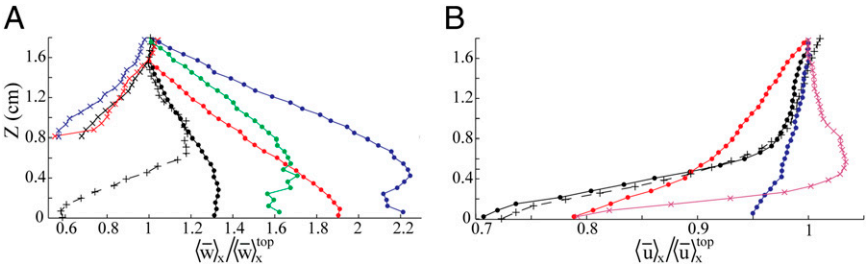

Fig. S2. Profiles of the vertical (*A*) and horizontal (*B*) mean velocity components normalized by the values measured 1.8 cm above *H. fuscescens* coral under different states of the polyps: extended and pulsating (full circles), contracted and inactive (× symbols), and extended but inactive (+ symbols). Z is the vertical axis with Z = 0 defined at the tip of the uppermost polyp seen in the corresponding UPIV images.

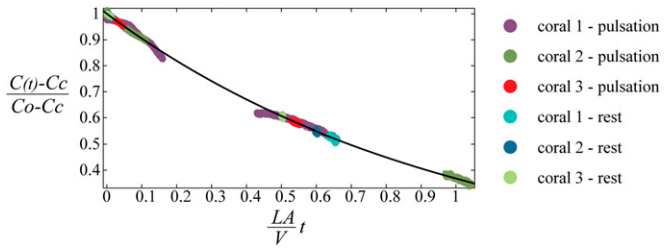

Fig. S3. Experimental results for the three *H. fuscescens* colonies (color coded) fitted to the exponential curve of Eq. **S2** in its dimensionless form (black line).

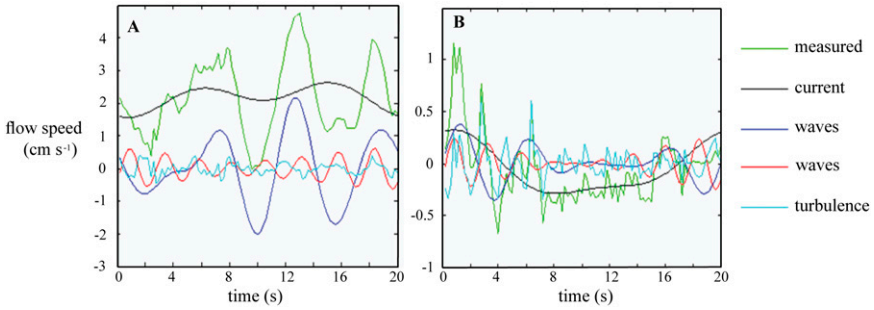

Fig. S4. Example of the measured (*A*) horizontal and (*B*) vertical velocities around an active coral, decomposed into the different velocity components by the FFT decomposition method.

Table S1. Measured and computed parameters obtained by the mass balance modeling

Parameter	Coral 1	Coral 2	Coral 3
V, cm^3	3,824	3,890	3,900
A pulsating, cm^2	1,224.6	1,601.4	1,318.8
A nonpulsating, cm^2	411.8	650.8	501.4
L pulsating, $cm \cdot min^{-1}$	0.0562	0.0256	0.0162
L nonpulsating, $cm \cdot min^{-1}$	0.0057	0.0022	0.0024
L ratio	9.86	11.63	6.77
Cc pulsating, $\mu mol \cdot L^{-1}$	500	590	800
Cc nonpulsating, $\mu mol \cdot L^{-1}$	600	666	1,000

Table S2. Gross photosynthesis to respiration ratio (P:R) in the pulsating *H. fuscescens* and in eight other nonpulsating corals reported in the literature

Species	Coral type	Pulsating	P:R	Source, ref. no.
Heteroxenia fuscescens	Soft	Yes	8.30	This study
Efflatounaria sp.	Soft	No	4.33	1
Xenia spp.*	Soft	No	5.08	1
Paralemnalia digitiformis	Soft	No	4.15	1
Capnella lacertiliensis	Soft	No	4.08	1
Sarcophyton spp.	Soft	No	4.77	1
Stylophora pistellata	Stony	No	2.77	2–4
Galaxea fascicularis	Stony	No	1.17	5
Montipora verrucosa	Stony	No	2.31	6
Acropora eurystoma	Stony	No	1.80	7

When several measurements were reported, we present an average ratio. All data presented are of corals in similar light intensities to our setting.
*These xeniid corals were not pulsating.

1. Fabricius KE, Klumpp DW (1995) Widespread mixotrophy in reef-inhabiting soft corals: The influence of depth, and colony expansion and contraction on photosynthesis. *Mar Ecol Prog Ser* 125(1–3):195–204.
2. Mass T, et al. (2007) Photoacclimation of *Stylophora pistillata* to light extremes: Metabolism and calcification. *Mar Ecol Prog Ser* 334:93–102.

3. Ferrier-Pages C, Gattuso JP, Dallot S, Jaubert J (2000) Effect of nutrient enrichment on growth and photosynthesis of the zooxanthellate coral *Stylophora pistillata*. *Coral Reefs* 19: 103–113.
4. Houlbreque F, Tmbutte E, Ferrier-Pages C (2003) Effect of zooplankton availability on the rates of photosynthesis, and tissue and skeletal growth in the scleractinian coral *Stylophora pistillata*. *J Exp Mar Biol Ecol* 296:145–166.
5. Al-Horani FA, Al-Moghrbi SM, de Beer D (2003) The mechanism of calcification and its relation to photosynthesis and respiration in the sclerctinian coral *Galaxea fascicularis*. *Mar Biol* 142:419–426.
6. Kinzie RA (1993) Effects of ambient levels of solar ultraviolet radiation of zooxanthellae and photosynthesis of the reef coral *Montipora verrucosa*. *Mar Biol* 116:319–327.
7. Schneider K, Erez J (2006) The effect of carbonate chemistry on calcification and photosynthesis in the hermatypic coral *Acropora eurystoma*. *Limnol Oceanogr* 51(3):1284–1293.

Table S3. UPIV database

Set no.	Coral ID	Polyp state	Mean U velocity, $cm \cdot s^{-1}$	Mean W velocity, $cm \cdot s^{-1}$
1	A	Active	−3.08	0.54
2	A	Active	−4.39	0.23
3	A	Active	−5.59	0.92
4	A	Active	−4.85	0.68
5	A	Not active	−4.69	2.70
6	A	Not active	−5.22	1.05
7	A	Not active, active geometry	7.92	0.45
8	B	Active	2.18	0.08
9	B	Active	2.46	0.25
10	B	Active	2.24	0.25
11	B	Active	1.62	0.21
12	B	Not active	−4.32	0.22
13	B	Not active	−5.11	1.85
14	B	Not active	−2.39	−0.04
15	B	Not active	−1.72	0.52
16	B	Not active	−3.56	0.98
17	B	Not active	−2.55	0.52

Listed are the conditions prevailing during all sets, including pulsation state and flow direction ∼2 cm above the coral interface. Each set includes 50–100 realizations.

Movie S1. Typical pulsation motions of the polyps of a *H. fuscescens* coral from the coral reef of Eilat, Red Sea.

Movie S1